ACS OMEGA

Open Access

This article is licensed under CC-BY-NC-ND 4.0

http://pubs.acs.org/journal/acsodf

Article

A New Framework for 3D Printing Aerogels with Additives: Hardware and Ink Development

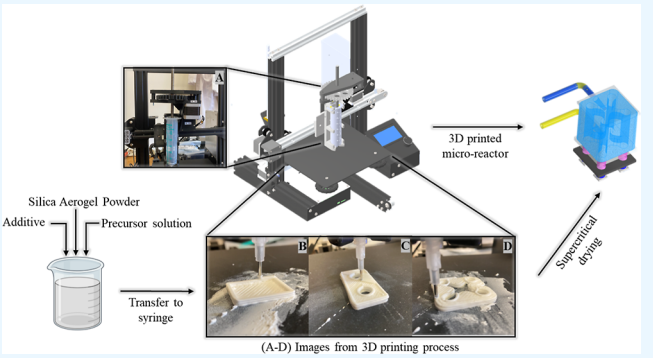
Jhan Luke Okkabaz, Saeid Darvishi, Işık Sena Akgün, Şansım Bengisu Barım, Ekin Özgönül, Defne Kuduğ, Çağla Parmaksızoğlu, Erkan Şenses, Can Erkey, and Alper Kiraz*

Cite This: *ACS Omega* 2026, 11, 340−348

Read Online

ACCESS | Metrics & More | Article Recommendations | Supporting Information

ABSTRACT: The 3D printing of functional aerogels, particularly those incorporating additives, represents a transformative approach in materials science, enabling the creation of highly customizable structures with advanced properties. This study introduces a 3D printing methodology for fabricating aerogel structures infused with titanium dioxide (TiO_2) nanoparticles, designed to enhance photocatalytic and environmental remediation applications. A commercially available 3D printer was adapted with a custom syringe pump system, allowing precise control over the extrusion of a shear-thinning aerogel ink. The ink formulation, tailored for compatibility with the system, achieved homogeneous dispersion of TiO_2 nanoparticles (55−230 nm) within the silica aerogel matrix at 50 wt % relative to silica content. Postprocessing steps, including gelation in ammonia vapor and supercritical CO_2 drying, preserved the intricate geometries of printed structures, which achieved a specific surface area of 407 m^2/g and a density of 0.15 g/cm^3. Rheological analysis demonstrated the ink's suitability for 3D printing, with viscosity decreasing from 10,000 Pa·s to 1 Pa·s under shear, enabling smooth extrusion due to shear thinning behavior, and elastic moduli confirming strong structural integrity necessary for retaining printed shapes. This approach enabled 3D printing of aerogel structures with <1 mm precision. It provides a scalable and cost-effective pathway for producing functional aerogels with tailored properties for potential applications in catalysis, thermal insulation, and environmental remediation.



(A-D) Images from 3D printing process

INTRODUCTION

Additive manufacturing, or 3D printing, is a transformative technology that has revolutionized diverse fields by enabling the creation of intricate structures through additive processes. This approach is particularly advantageous when developing complex materials and devices due to its precision, material efficiency, and scalability[1−4]. Among the wide array of materials explored for 3D printing, aerogels, a class of ultralight materials characterized by high porosity, low density, and large surface area, hold significant promise for advanced applications such as thermal insulation, catalysis, and environmental remediation.[5−8]

Aerogels are synthesized via sol−gel polymerization followed by drying to preserve their porous network. The combination of their exceptional properties and their ability to host functional nanoparticles has spurred interest in using them for photocatalytic applications.[9,10] Recent advancements have demonstrated the feasibility of integrating aerogel production with 3D printing to fabricate highly customizable aerogel architectures with tailored properties for specific uses.[3,8,11] These efforts have employed diverse printing methods, such as extrusion, photopolymerization, and template-assisted techniques, to achieve the resolution and material consistency required for practical applications.[12−16]

Despite these advancements, challenges remain in effectively combining the mechanical integrity and functionality of aerogels with the precision of 3D printing. Early studies showcased the potential of 3D-printed graphene aerogels for structural and catalytic applications.[3] Subsequent work explored silica aerogels produced via inkjet and extrusion methods, with notable applications in thermal management and environmental remediation.[8] However, the integration of optofluidic elements within 3D-printed aerogels remains underexplored, particularly for photocatalytic microreactors that leverage light-guiding capabilities for efficient pollutant degradation.[17]

This study addresses these gaps by introducing a novel 3D printing methodology to fabricate aerogel structures infused

Received: March 26, 2025
Revised: July 20, 2025
Accepted: August 26, 2025
Published: January 2, 2026



Downloaded via KOC UNIV on June 5, 2026 at 08:36:55 (UTC).
See https://pubs.acs.org/sharingguidelines for options on how to legitimately share published articles.

ACS Publications

© 2026 The Authors. Published by American Chemical Society

with titanium dioxide (TiO_2) nanoparticles. A modular 3D printing system was developed and optimized, including a tailored ink recipe and hardware modifications to ensure compatibility with the unique rheological properties of aerogel inks. While this study focused on creating stable and precise aerogel architectures, future work aims to incorporate parallel optofluidic waveguides within 3D-printed aerogels to guide UV light efficiently. This advancement would enhance photocatalytic degradation reactions, with phenol degradation serving as a widely recognized model to validate the performance and applicability of such microreactors. By leveraging the flexibility and precision of 3D printing, this study demonstrates a scalable pathway for producing advanced aerogel-based devices with potential applications in environmental and energy sectors.[18−20]

METHODS

3D Printer Hardware Design

This research addressed the material limitations of conventional fused deposition modeling (FDM) printers by designing a custom syringe pump to replace the traditional extruder. The commercially available Creality Ender 3 Pro 3D printer was selected for this project due to its low cost, modular design, and the adaptability of its parts, making it an ideal candidate for modification.[21]

Typically, 3D printers use Polylactic Acid (PLA) filament, a biodegradable thermoplastic derived from renewable resources like corn starch or sugar cane. The PLA filament, most commonly a 1.75 mm diameter wire, is extruded through a heated nozzle driven by a stepper motor. Although this setup is efficient for many applications, it is not suited to printing advanced and nonsolid materials like aerogel inks. To address these limitations, the standard extrusion components (extruder, heating element, and nozzle) were removed and replaced with a modular syringe pump system designed to handle the unique rheological properties of aerogel ink. This custom syringe pump integrated reused parts from the original printer, such as the extrusion stepper motor, nozzles, and screws, with newly fabricated components. Additional parts, including the syringe holder and cogs, were designed and 3D printed using an Ultimaker 2+, FMD-type printer chosen for its high resolution and reliability. This modification enabled precise control over the extrusion process, essential for high-resolution prints and maintaining the structural integrity of the aerogel structures while being easily replicable.

The syringe pump system uses a NEMA 17 stepper motor to drive syringes ranging from 10 to 50 mL, converting the motor's rotational motion into linear motion via a standard T8 lead screw and nut. This mechanism enables precise vertical movement of the syringe plunger, ensuring accurate extrusion of the aerogel ink. Additionally, ball bearings in the cogs minimize friction and ensure smooth operation, while the modular design allows for easy adjustments and maintenance, making it adaptable to various experimental needs.

The detailed components of the syringe pump system and their assembly are illustrated in Figure 1. This highlights the integration of reused and newly printed parts, showcasing the hybrid nature of the modified 3D printer. The development of this custom syringe pump system represents a significant advancement in the capability of FDM printers to handle novel materials like aerogels by making this customization a simple task.

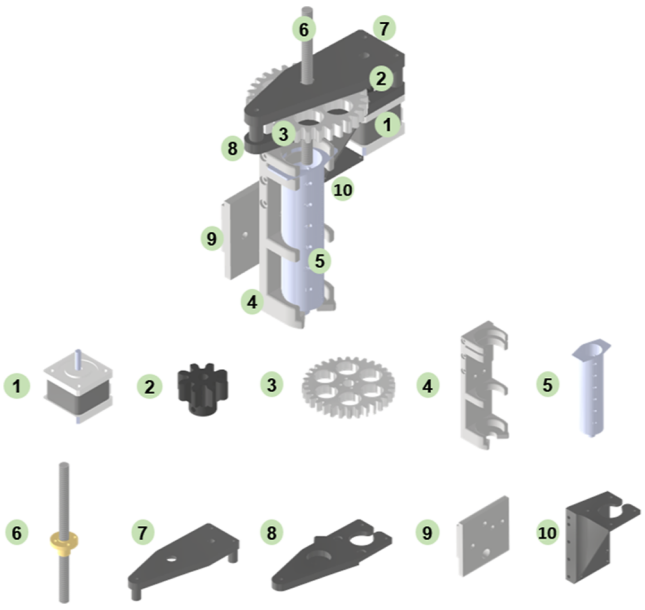


Figure 1. Syringe pump parts. (1) Stepper motor. (2) Driving cog. (3) Driven cog. (4) Syringe holder. (5) Syringe. (6) T8 Lead Screw. (7) Upper cog holder. (8) Lower cog holder. (9) Backplate. (10) Motor mount. Parts 2,3,4,7,8,9 and 10 were 3D printed with an Ultimaker 2+.

In addition to the main parts mentioned in Figure 1, two off-the-shelf 688Z 8 mm × 16 mm × 5 mm ball bearings were inserted into the upper and lower cog holders to reduce friction and allow the force to be efficiently applied. Standard hex socket M2 screws of varying lengths were used, enabling the entire syringe pump to be assembled and disassembled with a single M2 Allen key. The assembled syringe pump, shown in Figure 2, integrates these components, resulting in a robust and efficient mechanism for extruding aerogel ink. This modular design, combined with readily available components and custom 3D-printed parts, enhances the Creality Ender 3 Pro's capability to handle advanced materials like aerogels. This modification provides control over the extrusion process, which is essential for achieving high-resolution prints and maintaining the structural integrity of the printed aerogel structures.

All additional parts shown in Figure 2 were printed using PLA + at 205 °C with 30% infill and a 0.4 mm nozzle. PLA+ was chosen for its enhanced strength and flexibility compared to standard PLA. The infill was kept at 30% to reduce the weight on the printing arm, as higher weight could cause imprecise printing due to inertia during high-speed movements. Additional parts were 3D printed to address the wear of the small gear due to heat generation from the motor and friction between the small wheel and the motor pin.

The gear ratio in the presented design is optimized at 8:32 to achieve the best balance between printing speed and torque. A higher ratio increases torque and precision but reduces speed, while a lower ratio allows for faster printing with less force. This ratio can be adjusted based on the selected hardware and ink properties, ensuring optimal performance for different syringe sizes, viscosities, and print designs. Based on ink viscosity of 100 Pa·s and nozzle geometry, the estimated extrusion force required to maintain a flow rate of 3.24 cm^3/min was approximately 1.73 N (See supp. info. for further details). The aerogel ink is printed on glass slides (25 × 76 × 1

https://doi.org/10.1021/acsomega.5c02676
ACS Omega 2026, 11, 340−348

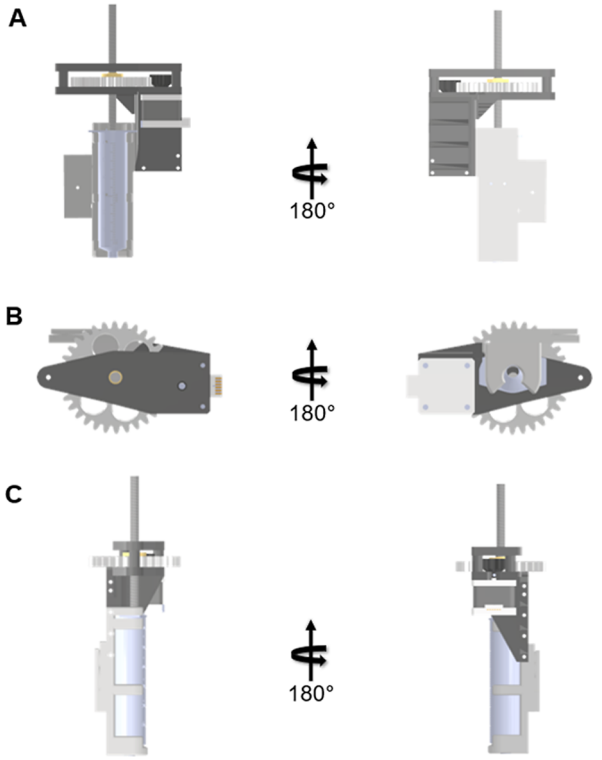


Figure 2. Assembled syringe pump. (A) Front, (B) top & bottom, (C) side view.

mm). These glass slides can be coated with lubricants, such as sunflower seed oil, to prevent damage during the removal of the aerogel structures.

A syringe needle set was obtained (Flumatic Fluid Control Equipment Co. Ltd.) and various syringe tips, including TE and TT dispensing tips ranging from 14 to 32 gauge, were tested to print geometries with different printing resolutions. The resulting print-out pictures can be included in the Supporting Information.

3D Printer Software and Calibration

On the software side, Cura Slicer, FullControl G-code Designer, and Repetier Host were utilized for data communication and G-code creation.[22,23] These programs are designed for filament-based FDM printers, which introduced challenges such as inadequate step size, incorrect gear rotation direction, and issues translating filament extrusion to ink extrusion parameters.[22,24] To address these problems, the initial G-code that sets the movement conditions had to be manually modified. This involved calculating the relationship between the stepper motor rotation and the vertical extrusion of the syringe pump.

A custom calibration software was developed in Python to automate this process. This software communicates with the printer via a USB port at 115200 bits per second to send G-code commands. The main features of this software, shown in Figure 3, include a manual G-code terminal to execute custom commands, linear movement control, motor step and speed control, an extrude and retract terminal, and a calibration terminal.

The calibration begins by setting an initial step value and filling the syringe with water. The water is extruded and weighed, and the weight is entered into the software to calculate a new step value. This process is repeated until the step value converges. This final step value is then used to modify the initial G-code so that the expected extrusion length matches the actual volume of extruded ink. Additionally, the software supports features such as cold extrusion, fan speed control, and print and bed temperature adjustments.

Although developed for thermoplastic extrusion systems, prior studies have demonstrated how tuning parameters like layer height and deposition conditions can significantly affect mechanical performance. We draw on this insight into emphasize the importance of process−structure relationships in our gel-based extrusion setup, where similar considerations such as nozzle geometry, extrusion rate, and interlayer spacing play a critical role in achieving mechanically robust aerogel structures.[25]

It should be noted that this calibration method is volumetric in nature and intended solely to align stepper motor

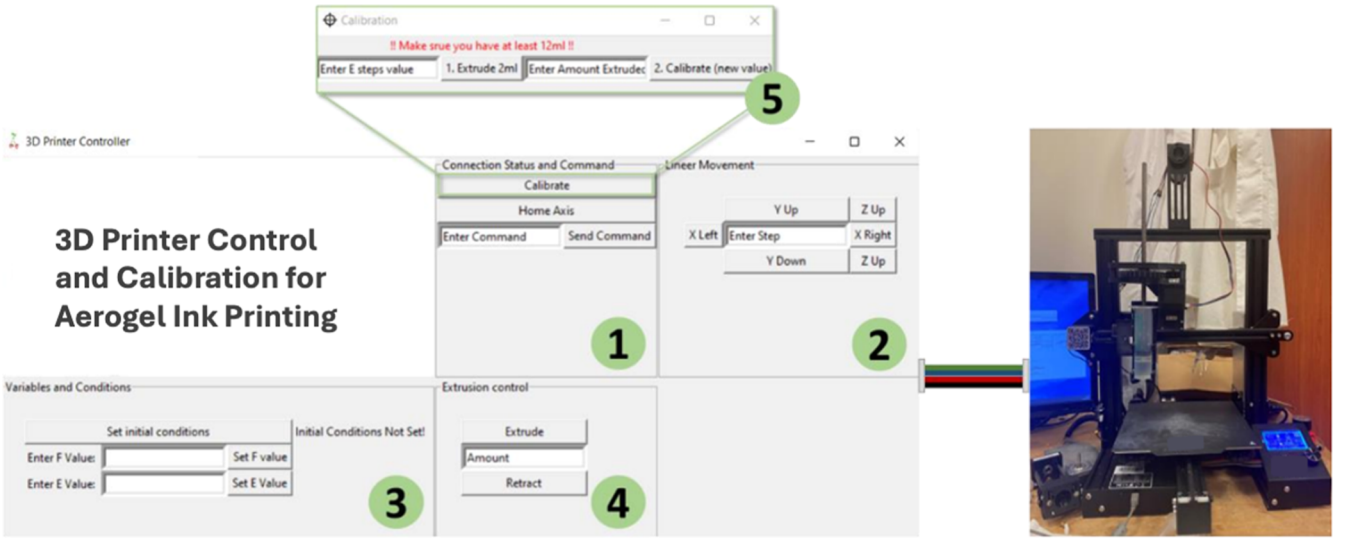


Figure 3. Manual calibration software. (1) Manual G-code terminal and calibration. (2) Linear movement control. (3) Motor step and speed control (4) extrude and retract terminal. (5) Calibration terminal.

https://doi.org/10.1021/acsomega.5c02676
ACS Omega 2026, 11, 340−348

Table 1. Silica Aerogel Ink Composition[a]

dynasylan-40 (ml)	1-pentanol (ml)	HNO_3 (μL)	water (ml)	aerogel particles (g)	PPGNH (ml)	TiO_2 (g)	HCl (μL)
2	11.2	5.2	0.16	0.86	0.73	0.7	0.1

[a]Recipe of materials for ink with TiO_2 as an additive.

displacement with the volume extruded; water is used as a Newtonian reference fluid to establish this step-to-volume relationship, independent of the rheological behavior of the printing ink.

Aerogel Ink Preparation

Prior to fabricating the aerogel structures, a printable ink was formulated based on previously established recipes, which we modified with targeted additives to tailor its properties for specific applications.[3,20] TiO_2 was chosen as an additive due to its excellent photocatalytic characteristics, promising for environmental remediation and other applications.[3,26]

Achieving printable aerogel inks requires tuning their rheological behavior. Specifically, the incorporation of silica particles introduces a yield stress and viscoelastic structure that enables shear-thinning extrusion and shape retention post-deposition, as established in prior work.[3,19]

The incorporation of TiO_2 aimed to explore its functional capabilities when embedded within the aerogel matrix. TiO_2's photocatalytic properties can potentially degrade organic pollutants and improve the efficiency of photocatalytic reactions, making it a valuable additive for aerogels used in environmental applications.[27,28]

The starter solution was composed of Dynasylan 40 (SiO_2 40−42 wt %) from Evonik Industries, 1-pentanol (ACS reagent, ≥99%), and nitric acid (HNO3, ACS reagent, 70%) from Sigma-Aldrich.[29] Initially, 2 mL of Dynasylan 40, 2.2 mL of 1-pentanol, and 0.16 mL of distilled water were mixed at 35 °C. After stirring at 250 rpm for 10 min, the mixture was allowed to cool to room temperature. Once cooled, 5.2 μL of HNO_3 was added via a micropipette and stirred for 5 min before being stored at 4 °C for 24 h. Table 1 shows the chemical composition of the solution.

After 24 h, the solution was brought back to room temperature. Concurrently, in another beaker, 9 mL of 1-pentanol and 0.73 mL of poly(propylene glycol) bis(2-aminopropyl ether) (PPGNH; Mn ≈ 4,000, Sigma-Aldrich) were mixed for 5 min at 500 rpm at room temperature. PPGNH was used to increase the viscosity, improve homogeneity, and prevent clumping when adding silica aerogel particles. Subsequently, 0.1 μL of hydrochloric acid (HCl, 37%; Sigma-Aldrich) was added. The solution was mixed at room temperature at 500 rpm for 5 min. Next, 0.86 g of silica aerogel particles (amorphous, 5−20 μm; IC3100) from Cabot Aerogel and 0.7 g of titanium dioxide (TiO_2) particles were added as the inclusion of silica particles contributes to the ink's yield stress and elastic modulus, which are necessary for extrusion and shape fidelity during 3D printing.[30] These amounts correspond to 100 and 50 wt % with respect to the SiO_2 content. Based on the densities of silica aerogel (0.12−0.15 g/cm^3) and TiO_2 (4.23 g/cm^3), and a total ink volume of approximately 14.1 mL, the solid volume fraction is estimated to fall within the range of 40%−50%. The mixture was then stirred at 1500 rpm for 5 min using a propeller to ensure homogeneity.

Following the extrusion process, the printed ink must undergo a gel transformation to form a rigid structure suitable for the drying process. Without gelation, the ink will not hold its shape during drying. Gelation was catalyzed by placing the printed structure in an airtight container which contains 1.7 mL of ammonia solution for 20 min. The amount of ammonia solution and the duration need to be adjusted depending on the thickness of the printed ink. Thicker prints may require up to 180 min. Once gelation was complete, the gel was immersed in a solution of 95% ethanol and 5% 2-propanol for 24 h to initiate the solvent exchange process. After the first 24 h, the solution was replaced with 100% ethanol and the process is repeated until solvent exchange is complete. Once the gel is free of 1-pentanol, it is placed in a 100 mL high-pressure vessel for supercritical drying.

To prevent the gelled aerogels from breaking during the drying process, paper meshes, such as tea bags, are used. Additionally, the vessel is filled with ethanol up to a volume of 100 mL, and then the gel is added to the vessel. This process uses the Applied Separations Speed SFE unit at 85 bar and 50 °C for 4 h. These parameters may vary depending on the printed structure. After this process, a 3D-printed TiO_2 silica aerogel structure is obtained, as shown in Figure 4.

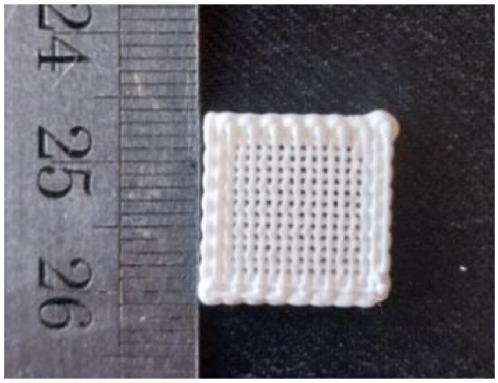


Figure 4. 3D printed grid aerogel structure with TiO_2 as an additive.

For applications requiring hydrophobic surfaces, a hexamethyldisilazane (HMDS) treatment can be used to modify the aerogel's surface chemistry, enhancing its performance in specific environments.[31] Notably, our findings, as demonstrated in Supplementary Figure S13, shows that the printed structures already exhibit a degree of hydrophobicity. However, HMDS treatment further enhances this property, making the aerogel even more suitable for targeted applications.

RESULTS AND DISCUSSION

Rheology

Rheological measurements on ink of silica-TiO_2 gel samples were conducted at 25 °C using a rheometer (Anton Paar MCR 302) with a 50 mm diameter, 2-degree cone geometry. Viscosity measurements were performed in a frequency sweep mode ranging from 0.01 to 1000 Hz. We selected cone−plate geometry to ensure uniform shear conditions across the

https://doi.org/10.1021/acsomega.5c02676
ACS Omega 2026, 11, 340−348

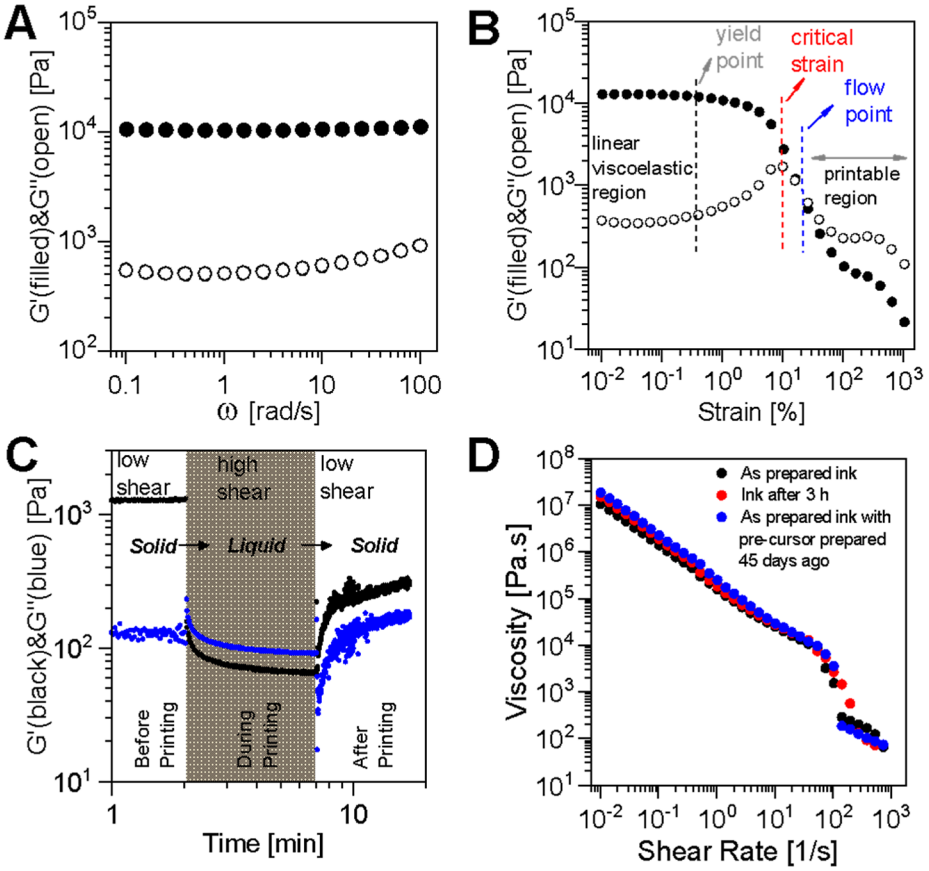


Figure 5. Rheological properties of the Silica/TiO_2 gel sample. (A) The storage (G′) and loss moduli (G″) of the Silica/TiO_2 gel sample. (B) The nonlinear storage modulus and viscous modulus of the ink. The gray line shows the yield point, red line indicates the critical strain, and the blue line indicates the flow point of the sample. (C) Ink recovery test. Storage, G′ (black) and viscous, G″ (blue) moduli of the silica/TiO_2 gel sample. Strain amplitude is in linear region (0.1%) in first 2 min and last 10 min. Strain amplitude is in nonlinear viscoelastic region (30%) from 2 to 7 min of the measurement. (D) Viscosity of the silica/TiO_2 gel sample with respect to the shear rate in three conditions. Back (as prepared), red (after 3 h) and blue (45 days after preparation).

sample, which is critical for probing nonlinear rheological behavior. The truncation gap (∼100 μm) was sufficiently larger than the particle size (5−20 μm), and no abnormal normal forces were observed which indicate minimal particle confinement and validating our choice. The ink exhibited shear-thinning behavior, essential for direct ink writing, allowing easy flow from the nozzle during printing and rapid viscosity increase postprinting to maintain the shape of the printed objects.

For small amplitude oscillatory shear (SAOS), an initial amplitude sweep test identified the linear viscoelastic region (LVR), followed by frequency sweep measurements from 0.1 to 100 rad/s. The linear viscoelastic modulus of the ink sample at 25 °C is shown in Figure 5A. Typical of gel-like materials, we observed G′ > G″ with parallel G′ and G″ behavior, indicating frequency-independent properties.

Large amplitude oscillatory shear (LAOS) tests were conducted at 1 rad/s angular frequency with strain amplitudes from 0.01% to 1000%. Transitioning from the SAOS-defined LVR to LAOS-induced nonlinear deformation provides insights into the material's microstructural properties and intermolecular interactions. Figure 5B displays the LAOS results. Initially, in the amplitude-independent regime, G′ gradually decreased with increasing strain amplitude at the LVR boundary, while G″ reached a maximum at critical strain (γc). Beyond γc, G″ decreased, indicative of weak strain overshoot or Type III behavior, with a peak defining critical strain, where gel network destruction outpaces reconstruction. Further strain led to both G′ and G″ declining, crossing at the "flow point," marking the transition from solid-like (elastic) to liquid-like (viscous) behavior, characterized by G″ > G′. Figure S14 in the Supporting Information presents the shear stress versus strain data obtained from LAOS measurements. From this data, the yield stress was determined to be 369.1 Pa. Based on this value, the minimum force required to initiate extrusion through a 1 mm diameter nozzle was estimated using $F = \tau \cdot A = 369.1\ \text{Pa} \times 7.854 \times 10^{-7}\ \text{m}^2 \approx 2.90 \times 10^{-4}$ N. The critical strain and flow point relate to the gel's deformability and structural strength.

Recovery tests were performed at strain amplitudes within the LVR and beyond the nonlinear region (>flow point). Initially, G′ and G″ of the aerogel sample were measured at 10 rad/s for 2 min within the LVR. Upon achieving a stable region, the strain amplitude was increased to 30%, resulting in liquid-like behavior with G″ > G′. After 5 min, measurements continued at lower strain amplitudes for 10 more minutes. Despite partial recovery of the loss modulus, the storage modulus did not fully recover after significant deformation in the second stage.

This partial recovery of the storage modulus (G′), along with the return to G′ > G″ as seen in Figure 5C, highlights the thixotropic nature of the ink. In this three-stage test, the ink

https://doi.org/10.1021/acsomega.5c02676
ACS Omega 2026, 11, 340−348

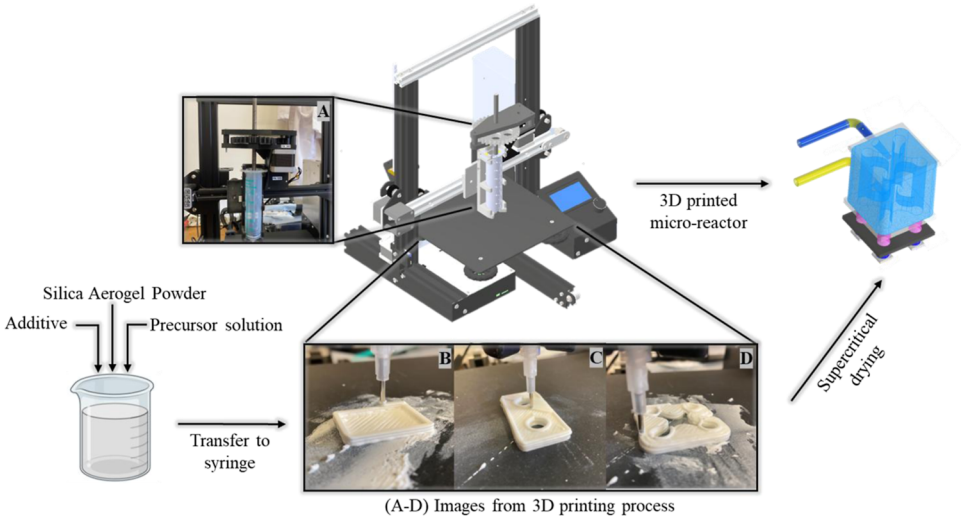


Figure 6. Process from ink production to microreactor.

first exhibits solid-like behavior ($G' > G''$) at low strain, simulating the resting condition of the ink before extrusion. Under high strain (30%), mimicking the extrusion process, the material transitions into a liquid-like state ($G'' > G'$), confirming a gel−sol transition required for flow. Upon returning to low strain, G' partially recovers, indicating that the ink can regain a solid-like structure after deformation. This reversible sol−gel behavior is critical to ensuring that the printed shape maintains structural fidelity postextrusion, before gelation occurs.[29,32,33]

Furthermore, Figure 5D demonstrates that the ink maintains sufficient viscosity over time, even after 3 h and up to 45 days postpreparation, reinforcing its long-term printability and consistent flow behavior. This temporal stability complements the yield stress and viscoelastic recovery observed in Figure 5C, confirming that the ink's structural stability is governed not solely by shear thinning but by the combination of yield stress, time-dependent recovery, and solid-like behavior at rest. These rheological properties enable the printed structures, as seen in Figures 6 and 8, to retain high fidelity throughout the printing and drying process.[34]

The rheology results demonstrate that our ink sample possesses the necessary mechanical properties for direct ink writing.[33,34] These specific mechanical properties allow the ink to flow easily from the nozzle during printing, with rapid viscosity increase postprinting to maintain the shape of the printed objects. These characterizations enable us to precisely print silica aerogel objects of various sizes and geometries.

3D Printing

The transformation of aerogel ink into functional structures involves a series of critical steps, beginning with ink preparation. Once formulated, the ink is promptly transferred to designated syringes to prevent solvent evaporation and maintain consistent rheology. Before printing, calibration is essential to optimize extrusion parameters. A glass slide is placed on the printing bed, serving as a substrate and facilitating easy transport to subsequent processing steps. Custom software streamlines calibration, while additional bed leveling, similar to standard FDM 3D printers, ensures precise layer deposition. The complete process, from ink preparation to the final microreactor structure, is outlined in Figure 6.

A primary issue encountered during the 3D printing process was the formation of macro and micro air pockets within the syringe during the ink loading process. These air pockets caused blockages and sudden ink extrusions, leading to inconsistencies during printing. Figure 7 illustrates the syringe before and after the air pocket removal process. The effects of these air pockets can be found in the Supporting Information.

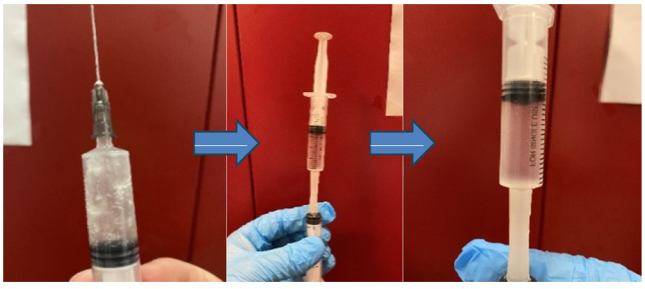


Figure 7. Air pocket removal process. The Left shows the syringe with air pockets. The Center is the air pocket removal setup while the right is the air pocket free ink.

The following processes were employed to remove the air pockets. Initially, the syringe containing the ink was oriented with the nozzle end upward and lightly tapped to allow large air pockets to rise to the surface. Standard syringe methods were used to eliminate these more oversized pockets. For smaller air pockets, an additional syringe connected via silicone tubing was utilized. A small puncture made in the tubing allowed air to escape without letting the ink pass through, ensuring a homogeneous ink mixture ready for consistent printing. These detailed steps in air pocket removal were crucial for achieving reliable and high-quality 3D prints, significantly improving the print quality and ensuring the structural integrity and precision of the aerogel structures.

Once the syringes are ready, the glass slides are positioned and secured, the desired nozzle size is attached, and the syringe is mounted to the pump. The printing process is then initiated. In our experiments, the maximum printed thickness tested was 1.2 mm, as our focus was on achieving high-resolution, structurally stable features rather than bulk structures.

https://doi.org/10.1021/acsomega.5c02676
ACS Omega 2026, 11, 340−348

Postprocessed Structures

The postprocessing of the printed aerogels involved several critical steps to ensure their final form and functionality. First, the gelation process was carried out by placing the 3D printed aerogels immediately in an ammonia vapor-filled chamber for 30 min to 3 h, depending on the wall thickness, to solidify the structures. Following gelation, the aerogels were carefully removed from their substrates and immersed in an isopropanol-ethanol solution for 24 h to begin the solvent exchange process. This was repeated with pure ethanol to replace the 1-pentanol, a necessary step before supercritical CO_2 drying. The drying process, conducted at 55 °C and 90 bar, ensured the preservation of the aerogels' delicate features and prevented shrinkage or collapse.[35] The final postprocessed structures, as seen in Figure 8, demonstrate the successful production of fine grid patterns and circular designs with submillimeter line lengths and intricate features, maintaining both structural integrity and precision. The printed structures were observed to remain stable in shape and mechanical integrity after solvent exchange and supercritical CO_2 drying.

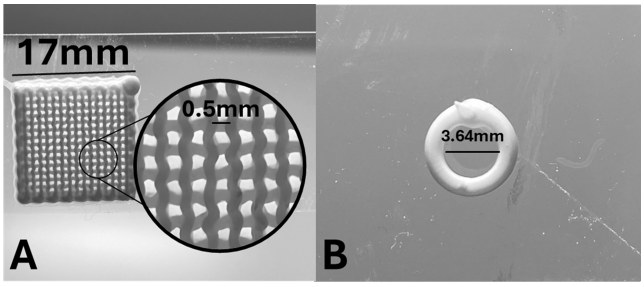


Figure 8. (A) Grid structure. (B) Cylindrical structure.

Surface Area and Density

To determine the surface area of the final structures, the aerogels were subjected to nitrogen adsorption/desorption analysis using a gas adsorption analyzer (ASAP 2020, Micromeritics). This analysis revealed a surface area of 407 m^2/g and a density of 0.15 g/cm^3. Additionally, a scanning electron microscope (SEM, Ultra Plus, ZEISS) was employed to examine the TiO_2 particle size and their dispersion within the aerogel. Figure 9 illustrates that the TiO_2 particles, ranging in size from 55 to 230 nm, are homogeneously dispersed within the aerogel network.[36]

CONCLUSION

The development and optimization of a 3D printing system for aerogels, particularly those with additives, represent a significant advancement in additive manufacturing and materials science. By modifying the 3D printer with a custom syringe pump and refining software for precise control, we overcame the limitations of conventional FDM printers, enabling the effective printing of nonsolid, highly viscous materials like aerogel ink. These modifications offer a low-cost and accessible solution for this novel application.

A critical challenge was the formation of air pockets within the syringe, which led to inconsistencies in the printed structures. Our systematic approach to removing these air pockets ensured a homogeneous ink mixture, leading to improved print reliability and structural integrity. Rheological characterization confirmed the shear-thinning behavior of the aerogel ink, which facilitated smoother extrusion and higher resolution in the printed structures.

The ability to incorporate additives like TiO_2 into the aerogel ink opens new avenues for functional applications.[37,38] TiO_2's photocatalytic properties enhance the aerogel's suitability for environmental remediation, catalysis, and other advanced applications. Surface area and density measurements, along with SEM analysis, validated the homogeneous dispersion of TiO_2 particles within the aerogel matrix, demonstrating the ink's effectiveness.

This research showcases the potential for scalable, high-resolution production of aerogels with tailored properties for specific applications. The customized 3D printer, equipped with a modular syringe pump and enhanced software, has proven capable of producing high-resolution and structurally robust aerogel constructs. These aerogels are suitable for a wide range of applications, including catalysis, thermal insulation, and environmental remediation.[39] Future research will focus on enhancing ink formulations with various additives, optimizing printing parameters, scaling up production, and exploring new functional applications such as photocatalytic microreactors.[40]

ASSOCIATED CONTENT

Data Availability Statement

The source code and hardware design files used for the 3D printer calibration and control, including the Python GUI and CAD components, are publicly available at:10.5281/zenodo.15485763

Supporting Information

The Supporting Information is available free of charge at https://pubs.acs.org/doi/10.1021/acsomega.5c02676.

Additional figures and data supporting the findings of this work are available in the Supporting Information. These include: photographs of the printing process and

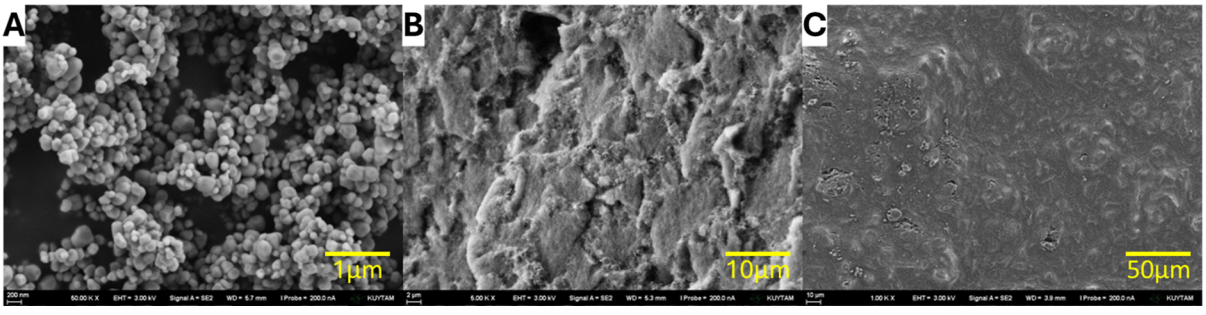


Figure 9. SEM images of TiO_2 particles and aerogel network. (A). TiO_2 particles. (B,C) Aerogel with TiO_2 particles at decreasing zoom levels.

https://doi.org/10.1021/acsomega.5c02676
ACS Omega 2026, 11, 340−348

postprocessed aerogel structures with and without TiO_2 additives (Figures S1−S5, S8−S12), effect of air pockets on printing (Figure S6), visual representation of the postprocessing workflow (Figure S7), contact angle measurements before and after surface treatment (Figure S13), and a quantitative estimation of the extrusion force required during printing, calculated using rheological data and fluid mechanics (S15) PDF)

AUTHOR INFORMATION

Corresponding Author

Alper Kiraz − *Department of Physics and Department of Electrical and Electronics Engineering, Koç University, Rumelifeneri Yolu, Istanbul 34450, Türkiye;* orcid.org/0000-0001-7977-1286; Email: akiraz@ku.edu.tr

Authors

Jhan Luke Okkabaz − *College of Science and Engineering, University of Minnesota, Minneapolis, Minnesota 55455, United States*

Saeid Darvishi − *Department of Chemical Engineering, Kocaeli University, Kocaeli 41001, Türkiye*

Işık Sena Akgün − *Department of Chemical and Biological Engineering, Koç University, Rumelifeneri Yolu, Istanbul 34450, Türkiye*

Şansım Bengisu Barım − *Department of Chemical and Biological Engineering, Koç University, Rumelifeneri Yolu, Istanbul 34450, Türkiye*

Ekin Özgönül − *Department of Physics, Koç University, Rumelifeneri Yolu, Istanbul 34450, Türkiye*

Defne Kuduğ − *Department of Chemical and Biological Engineering, Koç University, Rumelifeneri Yolu, Istanbul 34450, Türkiye; Department of Electrical and Electronics Engineering, Koç University, Rumelifeneri Yolu, Istanbul 34450, Türkiye;* orcid.org/0000-0002-6613-359X

Çağla Parmaksızoğlu − *Department of Electrical and Electronics Engineering, Koç University, Rumelifeneri Yolu, Istanbul 34450, Türkiye;* orcid.org/0009-0003-9203-4477

Erkan Şenses − *Department of Chemical and Biological Engineering, Koç University, Rumelifeneri Yolu, Istanbul 34450, Türkiye;* orcid.org/0000-0003-2593-1146

Can Erkey − *Department of Chemical and Biological Engineering, Koç University, Rumelifeneri Yolu, Istanbul 34450, Türkiye; Koç University Tüpraş Energy Center (KUTEM), Koç University, Rumelifeneri Yolu, Istanbul 34450, Türkiye;* orcid.org/0000-0002-2715-3299

Complete contact information is available at: https://pubs.acs.org/10.1021/acsomega.5c02676

Author Contributions

The project was initiated and coordinated by A.K.; The 3D printer hardware was designed and manufactured by J.L.O.; the custom calibration software was made by J.L.O.; the sample ink was prepared by J.L.O. with the help of I.S.A. and S.B.B.; the rheological testing and analysis was performed by S.D.; the data was interpreted by J.L.O., S.D., E.O., D.K., C.P., E.S., C.E., A.K.; the manuscript was written by J.L.O., C.E., and A.K.; all of the authors read and acknowledged the manuscript.

Notes

Figure Credits. All figures and photographs presented in this work were generated or captured by the authors.
The authors declare no competing financial interest.

ACKNOWLEDGMENTS

This work was supported by TÜBİTAK 1001 project (grant no: 121M497). A.K. acknowledges partial support from the Turkish Academy of Sciences (TÜBA).

REFERENCES

(1) Bhushan, B.; Caspers, M. An Overview of Additive Manufacturing (3D Printing) for Microfabrication. *Microsystem Technologies* **2017**, *23* (4), 1117−1124.

(2) Zhu, C.; Han, T. Y. J.; Duoss, E. B.; Golobic, A. M.; Kuntz, J. D.; Spadaccini, C. M.; Worsley, M. A. Highly Compressible 3D Periodic Graphene Aerogel Microlattices. *Nat. Commun.* **2015**, *6* (1), 6962.

(3) Zhao, S.; Siqueira, G.; Drdova, S.; Norris, D.; Ubert, C.; Bonnin, A.; Galmarini, S.; Ganobjak, M.; Pan, Z.; Brunner, S.; et al. Additive Manufacturing of Silica Aerogels. *Nature* **2020**, *584* (7821), 387−392.

(4) Rau, D. A.; Williams, C. P.; Bortner, M. J. Additive Manufacturing of Aerogels and Their Composites: Recent Advances, Challenges, and Future Outlook. *Prog. Mater. Sci.* **2023**, *140*, 101188.

(5) Fricke, J.; Emmerling, A. Aerogels. *J. Am. Ceram. Soc.* **1992**, *75* (8), 2027−2035.

(6) Pierre, A. C.; Pajonk, G. M. Chemistry of Aerogels and Their Applications. *Chem. Rev.* **2002**, *102* (11), 4243−4266.

(7) Wang, N.; Tan, F.; Wan, L.; Wu, M.; Zhang, X. Microfluidic Reactors for Visible-Light Photocatalytic Water Purification Assisted with Thermolysis. *Biomicrofluidics* **2014**, *8* (5), 054122.

(8) Zu, G.; Shen, J.; Wang, W.; Zou, L.; Lian, Y.; Zhang, Z. Silica−Titania Composite Aerogel Photocatalysts by Chemical Liquid Deposition of Titania onto Nanoporous Silica Scaffolds. *ACS Appl. Mater. Interfaces* **2015**, *7* (9), 5400−5409.

(9) Rechberger, F.; Niederberger, M. Synthesis of Aerogels: From Molecular Routes to 3-Dimensional Nanoparticle Assembly. *Nanoscale Horizons* **2017**, *2* (1), 6−30.

(10) Moner-Girona, M.; Roig, A.; Molins, E.; Llibre, J. Sol-Gel Route to Direct Formation of Silica Aerogel Microparticles Using Supercritical Solvents. *J. Sol-Gel Sci. Technol.* **2003**, *26* (1−3), 645−649.

(11) Feng, J.; Su, B.-L.; Xia, H.; Zhao, S.; Gao, C.; Wang, L.; Ogbeide, O.; Feng, J.; Hasan, T. Printed Aerogels: Chemistry, Processing, and Applications. *Chem. Soc. Rev.* **2021**, *50* (6), 3842−3888.

(12) He, P.; Tang, X.; Chen, L.; Xie, P.; He, L.; Zhou, H.; Zhang, D.; Fan, T. Patterned Carbon Nitride−Based Hybrid Aerogel Membranes via 3D Printing for Broadband Solar Wastewater Remediation. *Adv. Funct. Mater.* **2018**, *28* (29), 1801121.

(13) Sun, D.; Liu, W.; Tang, A.; Guo, F.; Xie, W. A New PEGDA/CNF Aerogel-Wet Hydrogel Scaffold Fabricated by a Two-Step Method. *Soft Matter* **2019**, *15* (40), 8092−8101.

(14) Teo, N.; Joo, P.; Amis, E. J.; Jana, S. C. Development of Intricate Aerogel Articles Using Fused Filament Fabrication. *ACS Appl. Polym. Mater.* **2019**, *1* (7), 1749−1756.

(15) Yarahmadi, M.; Barcelona, P.; Fargas, G.; Xuriguera, E.; Roa, J. J. Optimization of the ceramic ink used in Direct Ink Writing through rheological properties characterization of zirconia-based ceramic materials. *Ceram. Int.* **2022**, *48* (4), 4775−4781.

(16) Tetik, H.; Wang, Y.; Sun, X.; Cao, D.; Shah, N.; Zhu, H.; Qian, F.; Lin, D. Additive Manufacturing of 3D Aerogels and Porous Scaffolds: A Review. *Adv. Funct. Mater.* **2021**, *31* (52), 2103410.

(17) Smirnova, I.; Gurikov, P. Aerogels in Chemical Engineering: Strategies Toward Tailor-Made Aerogels. *Annu. Rev. Chem. Biomol. Eng.* **2017**, *8*, 307−334.

(18) Eris, G.; Sanli, D.; Ulker, Z.; Bozbag, S. E.; Jonás, A.; Kiraz, A.; Erkey, C. Three-Dimensional Optofluidic Waveguides in Hydro-

phobic Silica Aerogels via Supercritical Fluid Processing. *J. Supercrit. Fluids* **2013**, *73*, 28−33.
(19) Özbakır, Y.; Jonas, A.; Kiraz, A.; Erkey, C. Aerogels for Optofluidic Waveguides. *Micromachines* **2017**, *8* (4), 98.
(20) Özbakır, Y.; Jonáš, A.; Kiraz, A.; Erkey, C. An Aerogel-Based Photocatalytic Microreactor Driven by Light Guiding for Degradation of Toxic Pollutants. *Chem. Eng. J.* **2021**, *409*, 128108.
(21) Baas, S.; Saggiomo, V. Ender3 3D Printer Kit Transformed into Open, Programmable Syringe Pump Set. *HardwareX* **2021**, *10*, No. e00219.
(22) Gleadall, A. FullControl GCode Designer: Open-Source Software for Unconstrained Design in Additive Manufacturing. *Addit. Manuf* **2021**, *46*, 102109.
(23) Gomez Alonso, J. L.; Allue Salvador, A.; De Marco Rodriguez, I.; Retolaza Gaviña, J.; Diez Barcenilla, G.; Barcenilla, G. D. Influence Of Slicer Software Used With 3d Printing Filament Extrusion Technology On Properties Of Printed Parts With Short Fiber Reinforced Thermoplastic Composite. *DYNA* **2022**, *97* (3), 295−300.
(24) Wei, P.; Cipriani, C.; Hsieh, C.-M.; Kamani, K.; Rogers, S.; Pentzer, E. Go with the flow: Rheological requirements for direct ink write printability. *J. Appl. Phys.* **2023**, *134* (10), 055105.
(25) Garzon-Hernandez, S.; Garcia-Gonzalez, D.; Jérusalem, A.; Arias, A. Design of FDM 3D Printed Polymers: An Experimental-Modelling Methodology for the Prediction of Mechanical Properties. *Mater. Des.* **2020**, *188*, 108414.
(26) Štengl, V.; Bakardjieva, S.; Šubrt, J.; Szatmary, L. Titania Aerogel Prepared by Low Temperature Supercritical Drying. *Microporous Mesoporous Mater.* **2006**, *91* (1−3), 1−6.
(27) Chen, X.; Ye, X.; He, J.; Pan, L.; Xu, S.; Xiong, C. Preparation of Fe3+-Doped TiO2 Aerogels for Photocatalytic Reduction of CO2 to Methanol. *J. Sol-Gel Sci. Technol.* **2020**, *95* (2), 353−359.
(28) Wang, J.; Shi, Z.; Gong, J.; Zhou, X.; Li, J.; Lyu, Z. 3D Printing of Graphene-Based Aerogels and Their Applications. *FlatChem.* **2024**, *47*, 100731.
(29) Maleki, H.; Durães, L.; Portugal, A. An Overview on Silica Aerogels Synthesis and Different Mechanical Reinforcing Strategies. *J. Non-Cryst. Solids* **2014**, *385*, 55−74.
(30) Truby, R. L.; Lewis, J. A. Printing Soft Matter in Three Dimensions. *Nature* **2016**, *540* (7633), 371−378.
(31) Malfait, W. J.; Zhao, S.; Verel, R.; Iswar, S.; Rentsch, D.; Fener, R.; Zhang, Y.; Milow, B.; Koebel, M. M. Surface Chemistry of Hydrophobic Silica Aerogels. *Chem. Mater.* **2015**, *27* (19), 6737−6745.
(32) Menshutina, N.; Abramov, A.; Tsygankov, P.; Lovskaya, D. Extrusion-Based 3D Printing for Highly Porous Alginate Materials Production. *Gels* **2021**, *7* (3), 92.
(33) Hyun, K.; Kim, S. H.; Ahn, K. H.; Lee, S. J. Large Amplitude Oscillatory Shear as a Way to Classify the Complex Fluids. *J. Non-Newtonian Fluid Mech.* **2002**, *107* (1−3), 51−65.
(34) Şahin, İ.; Özbakır, Y.; İnönü, Z.; Ulker, Z.; Erkey, C. Kinetics of Supercritical Drying of Gels. *Gels* **2017**, *4* (1), 3.
(35) García-González, C. A.; Camino-Rey, M. C.; Alnaief, M.; Zetzl, C.; Smirnova, I. Supercritical Drying of Aerogels Using CO2: Effect of Extraction Time on the End Material Textural Properties. *J. Supercrit. Fluids* **2012**, *66*, 297−306.
(36) Chen, T.; Sun, A.; Chu, C.; Wu, H.; Wang, J.; Wang, J.; Li, Z.; Guo, J.; Xu, G. Rheological behavior of titania ink and mechanical properties of titania ceramic structures by 3D direct ink writing using high solid loading titania ceramic ink. *J. Alloys Compd.* **2019**, *783*, 321−328.
(37) Liu, M.; Gan, L.; Pang, Y.; Xu, Z.; Hao, Z.; Chen, L. Synthesis of Titania−Silica Aerogel-like Microspheres by a Water-in-Oil Emulsion Method via Ambient Pressure Drying and Their Photocatalytic Properties. *Colloids Surf., A* **2008**, *317* (1−3), 490−495.
(38) Duan, J.; Li, Q.; Xu, W.; Hu, X.; Wang, Y.; Valdez, S. M.; Qiang, Z.; Liao, Y.; Wen, J.; Ye, C.; et al. Mechanically Flexible and Weavable Hybrid Aerogel Fibers with Ultrahigh Metal−Organic Framework Loadings for Versatile Applications. *ACS Appl. Polym. Mater.* **2024**, *6* (3), 1900−1910.
(39) Gusain, R.; Kumar, N.; Ray, S. S. 3D-Printed Hydrogels and Aerogels for Water Treatment and Energy Storage Applications. *ChemistrySelect* **2023**, *8* (20), No. e202300738.
(40) Payanda Konuk, O.; Alsuhile, A. A. A. M.; Yousefzadeh, H.; Ulker, Z.; Bozbag, S. E.; García-González, C. A.; Smirnova, I.; Erkey, C. The effect of synthesis conditions and process parameters on aerogel properties. *Frontiers in Chemistry* **2023**, *11*, 1294520.



https://doi.org/10.1021/acsomega.5c02676
ACS Omega 2026, 11, 340−348